Chemical Engineering Science 66 (2011) 5899–5909

Contents lists available at SciVerse ScienceDirect

Chemical Engineering Science

journal homepage: www.elsevier.com/locate/ces

Numerical study of condensing bubble in subcooled boiling flow using volume of fluid model

Seong-Su Jeon [a], Seong-Jin Kim [b], Goon-Cherl Park [a,*]

[a] Department of Nuclear Engineering, Seoul National Univ., San 56-1, Sillim-dong, Gwanak-gu, Seoul 151-744, Republic of Korea
[b] Korea Atomic Energy Research Institute, 1045 Daedeokdaero, Yuseong-gu, Daejeon 305-600, Republic of Korea

ARTICLE INFO

Article history:
Received 3 March 2011
Received in revised form
31 July 2011
Accepted 6 August 2011
Available online 12 August 2011

Keywords:
Bubble behavior
Condensation
Heat and mass transfer
Two-phase flow
Numerical analysis
VOF model

ABSTRACT

In this numerical study, the behavior of condensing bubble was investigated using the volume of fluid (VOF) model in the FLUENT code. In order to simulate the condensing bubble with the FLUENT code, the bubble condensation was modeled using the user-defined function (UDF). For the validation of the UDF of bubble condensation, the results of CFD simulation were compared with the results of a bubble condensation experiment performed in Seoul National University (SNU). Simulation results showed good agreements with the experimental data. Moreover, the fundamental behavior of the condensing bubble was investigated in various conditions. The effects of condensation on bubble behavior were analyzed by comparing the behavior of condensing bubbles with that of adiabatic bubbles. It was found that the behavior of the condensing bubble was different from that of the adiabatic bubble in many respects including the bubble shape, velocity, rise distance and moving trajectory.

1. Introduction

Subcooled boiling flows are encountered in many industrial applications such as boilers, nuclear reactors, and the new generation of electronic and computer systems. There have been many efforts to understand and model subcooled boiling flow. In the field of nuclear engineering, subcooled boiling flows have been studied as an important issue in the optimum design and safety of nuclear systems because the presence of vapor bubbles has a large effect on the heat transfer characteristics of a nuclear system as well as pressure drops, flow instability, etc. However, subcooled boiling flow is very difficult to understand due to the complex behavior of bubbles with heat and mass transfer through the bubble interface. Therefore, in order to understand subcooled boiling flow, which is a challenging problem, it is essential to acquire thorough knowledge on condensing bubbles.

There have been many experimental analyses on bubble behavior. In these experimental studies, bubble behavior regarding the bubble size, shape, velocity and moving trajectory was investigated in various conditions. However, it has been impossible to obtain complete information about the bubble behavior due to the existence of the bubble interface between the vapor and liquid phases. The shape and the area of the varying interface, which governs the behavior of each phase, are very complex and thus difficult to measure. Moreover, in subcooled boiling flow, bubble condensation significantly affects the change of interface so this complicates the analysis of the behavior of condensing bubbles even more. Therefore, it is necessary to carry out numerical simulations for bubble behavior as a complement to experiments. Such numerical simulations may contribute to a better physical understanding of complex phenomena regarding the behavior of condensing bubbles.

One of the numerical methods for bubble simulation is the volume of fluid (VOF) model proposed by Hirt and Nichols (1981). It can deal with immiscible fluids with clearly defined interface; the direct simulation of the varying interface is possible. Many numerical studies have analyzed bubble behavior in terms of the bubble size, bubble shape, rise trajectory and bubble velocity using the VOF model. Tomiyama et al. (1991a), Wachem and Schouten (2002), Lörstad and Fuchs (2004), and Gopala and Wachem (2008) examined the applicability of the VOF model to the analysis of a single rising bubble in liquid. These examinations confirmed that the VOF model can yield good predictions of the bubble shape and terminal velocity. The VOF model also has been used to analyze the following: the effect of a channel wall on bubble shapes and terminal velocities (Tomiyama et al., 1991b); the velocity distribution and the distribution of the local wall shear stress in slug flow (Taha and Cui, 2006); the effect of the liquid velocity field on bubble motion in a linear shear flow (Tomiyama et al. 1993); the trajectories of bubbles with various

* Corresponding author. Tel.: +82 2 880 7210; fax: +82 2 889 2688.
E-mail address: parkgc@snu.ac.kr (G.-C. Park).

0009-2509/$ - see front matter © 2011 Elsevier Ltd. All rights reserved.
doi:10.1016/j.ces.2011.08.011

initial diameters that rise in water (Krishna and Baten, 1999); the coalescence of two gas bubbles (Chen and Li, 1998; Annaland et al. 2005); the effect of the bubble size/shape and neighboring bubbles on the magnitude and direction of the lift force (Rabha and Buwa, 2009); etc. The simulation results showed good agreements with the experimental data. However, most bubble simulations were limited to cases of adiabatic systems such as air bubble-water flow, where the heat and mass transfer between each phase were not considered. Those simulation results for bubble behavior are only valid for analyzing bubble behavior in adiabatic systems.

However, in subcooled boiling flow, bubble condensation is the key parameter to describe heat and mass transfer phenomena. It significantly affects the shape and the area of the varying interface thus the behavior of the condensing bubble becomes different from that of the adiabatic bubble. Therefore, in order to understand bubble behavior in subcooled boiling flow, a numerical study of condensing bubbles considering heat and mass transfer through the bubble interface is required.

This study focused on how to simulate bubble condensation with a CFD code. Moreover, using the VOF model, the behavior of condensing bubbles in subcooled boiling flow was investigated. In order to simulate the condensing bubble with the FLUENT code, the bubble condensation was modeled using the user-defined function (UDF). For the validation of the UDF of bubble condensation, the results of CFD simulation were compared with the SNU experimental results. Through the VOF model coupled with the UDF of bubble condensation, the fundamental behavior of condensing bubble in terms of the bubble velocity, rise distance and moving trajectory was investigated under various conditions. The effects of condensation on bubble behavior were analyzed by comparing the behavior of condensing bubbles with that of adiabatic bubbles.

2. VOF model

In this study, the volume of fluid (VOF) model in a commercial CFD code FLUENT 6.2.16 (2001) is used to simulate condensing bubbles in subcooled boiling flow. The gas and liquid phases are considered as incompressible fluids and the flow is assumed to be laminar.

In the VOF model, the governing equations are solved using the volume fraction in each cell. A particular phase, '*k*', is identified by its volume fraction, α_k, in a computational cell. For $\alpha_k=1.0$, the cell is full of the secondary phase. For $\alpha_k=0.0$, the cell is full of the primary phase. For $0.0<\alpha_k<1.0$, the cell contains the interface between the primary and secondary phases. In each control volume, the volume fractions of all phases, i.e., α_k for all k, sum to unity

$$\sum_{k=1}^{n}\alpha_k=1 \tag{1}$$

Fig. 1 shows the sample calculation of volume fraction in each cell in this bubble simulation. For $\alpha_g=1.0$ and $\alpha_g=0.0$, the cell represents the vapor and liquid regions, respectively. For $0.0<\alpha_g<1.0$, the cell represents the interface region. A free-surface of the bubble is in the interface region. In this study, a bubble is defined as an aggregate composed of cells where volume fractions are in the range of $0.0<\alpha_g\leq 1.0$.

The tracking of the interface between the phases is accomplished by the solution of a continuity equation for the volume fraction of any of the phases. For the kth phase, the volume fraction equation has the following form:

$$\frac{\partial\alpha_k}{\partial t}+\vec{v}\nabla\alpha_k=\frac{S_{\alpha_k}}{\rho_k} \tag{2}$$

where S_{α_k} is the mass source term. In this study, this mass source term is modeled to simulate mass transfer between the phases during condensation.

The fields for all variables and properties are shared by the phases. Based on the local volume fraction, α_k, the appropriate properties and variables will be assigned to each control volume within the domain. In a two-phase system, if the phases are represented by the subscripts, 1 and 2, and if the volume fraction of the second of these is being tracked, the density in each cell is

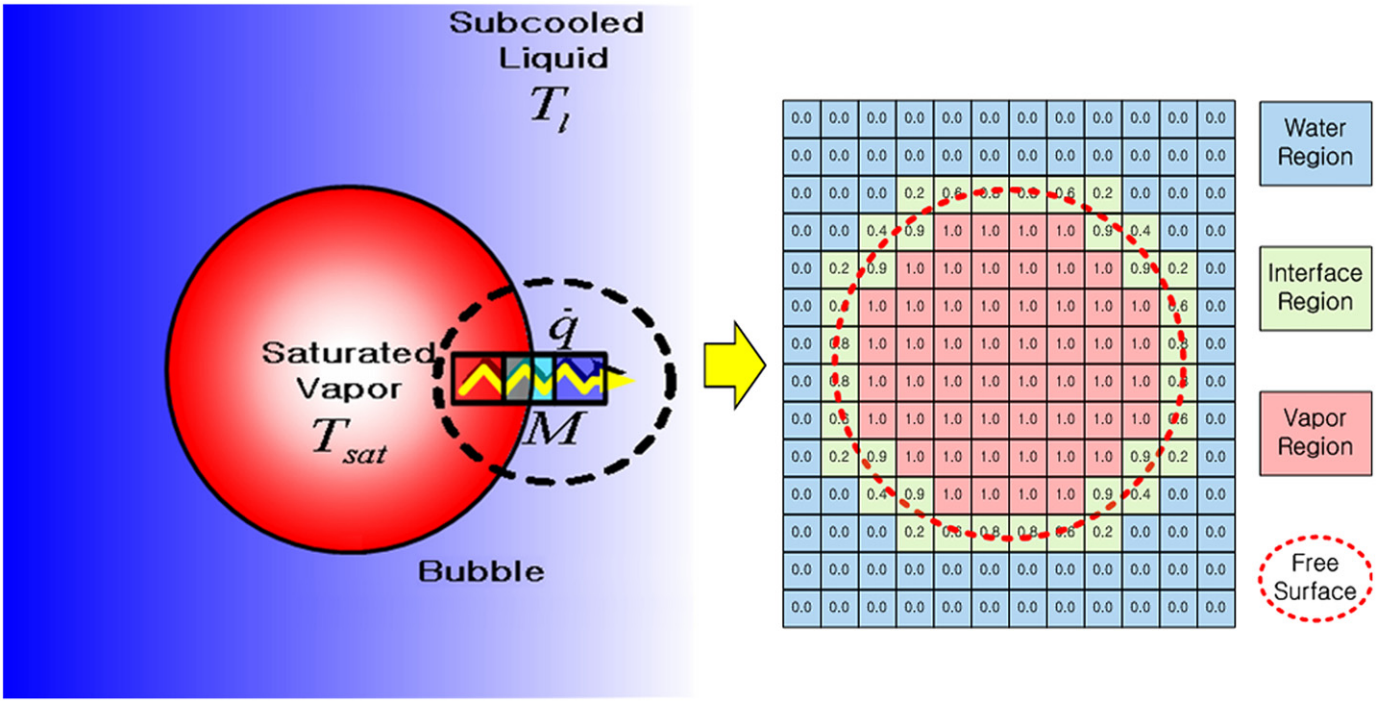

Fig. 1. A sample calculation of volume fraction in each cell using VOF model.

determined as follows:

$$\rho = \alpha_2\rho_2 + (1-\alpha_2)\rho_1 \tag{3}$$

All the other properties (e.g., viscosity) are computed in this manner.

In the VOF model, a single momentum equation for an incompressible flow is solved throughout the domain, and the obtained velocity field is shared among the phases. The momentum equation shown in Eq. (4) depends on the volume fractions of all the phases through the properties, ρ and μ

$$\frac{\partial}{\partial t}(\rho\vec{v}) + \nabla(\rho\vec{v}\,\vec{v}) = -\nabla p + \nabla\left[\mu(\nabla\vec{v} + \nabla\vec{v^T})\right] + \rho\vec{g} + \vec{F} \tag{4}$$

In Eq. (4), v is treated as a mass-averaged variable

$$v = \frac{\alpha_1\rho_1 v_1 + \alpha_2\rho_2 v_2}{\rho} \tag{5}$$

In the momentum equation, the accumulation and convective momentum terms in every cell balance the pressure forces, shear forces, gravitational body forces and additional forces, $\vec{F}$, which may be added depending upon the problem. In this bubble simulation, $\vec{F}$ is the surface tension force per unit volume.

The energy equation, also shared among the phases, is shown below

$$\frac{\partial}{\partial t}(\rho E) + \nabla(\vec{v}(\rho E + p)) = \nabla(k_{eff}\nabla T) + S_h \tag{6}$$

The VOF model treats the energy, E, and temperature, T, as mass-averaged variables

$$E = \frac{\sum_{k=1}^{n}\alpha_k\rho_k E_k}{\sum_{k=1}^{n}\alpha_k\rho_k} \tag{7}$$

In the above, E_k for each phase is based on the specific heat of that phase and the shared temperature. Both ρ and k_{eff} are shared by the phases. The source term, S_h, is for the volumetric heat source. In this study, this energy source term is modeled to simulate heat transfer between the phases during condensation.

Summarizing, in the vapor- and water-cells, the governing equations are solved for only the vapor and liquid phases, respectively. However, in the interface-cell, governing equations are solved for the mixture phase. It should be noted that source terms exist only in the governing equations of the interface-cell. Using these governing equations, it is possible to simulate the complex change of the bubble interface.

3. Modeling of bubble condensation

Using the default VOF model in the FLUENT code, the adiabatic bubble behavior can be simulated. However, the source terms in the governing equations should be modeled to simulate bubble condensation because the default VOF model cannot simulate heat and mass transfer through the bubble interface.

In this study, the user-defined function (UDF) of FLUENT is used to model the source terms. The UDF is a routine written in the C programming language and is based on the FLUENT macro, which can be dynamically linked with the FLUENT solver. It can be programmed by the user. It is possible to define user's own initial and boundary conditions and source terms. The modeling procedure for UDF of bubble condensation is as follows.

3.1. Modeling of interfacial heat transfer coefficient

In order to model the bubble condensation, this study uses Eq. (8) for the convective heat and mass transfer

$$\dot{q} = h_i A_b(T_{sat} - T_l) = \dot{M}h_{fg} \tag{8}$$

where h_i is the interfacial heat transfer coefficient (IHTC), T_{sat} and T_l are the vapor and liquid temperatures, respectively, A_b is the interfacial- or surface area of the bubble, $\dot{M}$ is the total mass transfer rate and h_{fg} is the latent heat.

In Eq. (8), it is necessary to first model the IHTC. In order to calculate the IHTC, this study uses the condensation correlation obtained from the SNU experiment on single bubble condensation (Kim and Park, 2011) as shown in Eq. (9). This is because the experiment is used for the validation of this UDF of bubble condensation later

$$Nu_c = \frac{h_i D_s}{k_l} = 0.2575 Re_b^{0.7} Ja_l^{-0.2043} Pr_l^{-0.4564} \tag{9}$$

The calculations for each parameter in Eq. (9) are shown below.

First, the bubble Reynolds number (Re_b) is defined as:

$$\mathrm{Re}_b = \frac{\rho_l U_{rel} D_s}{\mu_l} \tag{10}$$

where ρ_l, U_{rel}, D_s and μ_l are the liquid density, bubble relative velocity, bubble Sauter diameter and liquid viscosity, respectively.

In Eq. (10), the bubble relative velocity (U_{rel}) is defined as

$$U_{rel} = \sqrt{(U_{b,x})^2 + (U_{b,y})^2 + (U_{b,z} - U_{l,z})^2} \tag{11}$$

where $U_{b,x}$, $U_{b,y}$ and $U_{b,z}$ are the instantaneous absolute bubble velocities in the transverse (x), normal (y) and axial (z) directions, respectively. $U_{l,z}$ is the local liquid velocity. The bubble velocity is calculated by computing the change of the center of mass for the bubbles at each time-step.

The center of mass (X_{CM}) for the bubbles is defined as

$$X_{CM} = \frac{\sum_j \alpha_{g,j}\rho_g V_j x_{CM,j}}{\sum_j \alpha_{g,j}\rho_g V_j} \tag{12}$$

where $\alpha_{g,j}$ is the vapor volume fraction in the jth cell, V_j is the volume of the jth cell, ρ_g is the vapor density and $x_{CM,j}$ denotes the center coordinates in the jth cell.

In Eq. (10), the bubble Sauter diameter (D_s) is defined as

$$D_s = 6.0\frac{V_b}{A_b} \tag{13}$$

where V_b is the bubble volume calculated from the relation: $\sum_j \alpha_{g,j}V_j$. A_b is the bubble surface area. Since a free-surface of the bubble is in the interface region (see Fig. 1), this study defines the bubble surface as the iso-surface that has a mean volume fraction, $\alpha_g = 0.5$, and calculates the bubble surface area using the area of the iso-surface.

By substituting Eqs. (11) and (13) into Eq. (10), the bubble Reynolds number is obtained.

Second, the Jakob number (Ja) is defined as

$$Ja_l = \frac{\rho_l C_{pl}(T_{sat} - T_l)}{\rho_g h_{fg}} \tag{14}$$

where T_l is the local liquid temperature at the center of mass for the bubble in the liquid temperature profile and C_{pl} is the liquid specific heat.

Third, the Prandtl number (Pr) is defined as

$$\mathrm{Pr}_l = \frac{C_{pl}\mu_l}{k_l} \tag{15}$$

where k_l is the liquid thermal conductivity. In this study, the Prandtl number is constant because it is just a function of liquid properties assumed as constant and is not related to bubble behavior.

Finally, IHTC is obtained by applying Eqs. (10), (14) and (15) in the condensation correlation, Eq. (9).

3.2. Modeling of source terms

The source terms are modeled using h_i calculated from Eq. (9). The procedure to model the source terms is as follows.

From Eq. (8), the total mass transfer rate from vapor to liquid is obtained as

$$\dot{M} = \frac{\dot{q}}{h_{fg}} = \frac{h_i A_b (T_{sat} - T_l)}{h_{fg}} \tag{16}$$

Because the total mass transfer rate is defined as the sum of mass transfer rate in each interface-cell, the total mass transfer rate is rewritten as

$$\dot{M} = \sum_j \dot{m}_j V_j = \sum_j \alpha_{g,j} \dot{m} V_j \tag{17}$$

where $\dot{m}$ is the average mass transfer rate, i.e., the overall mass transfer rate divided by the total vapor volume in the bubble interface region

$$\dot{m} = \frac{\dot{M}}{\sum_j \alpha_{g,j} V_j} \tag{18}$$

$\dot{m}_j$ is the mass transfer rate in the jth interface-cell

$$\dot{m}_j = \alpha_{g,j} \dot{m} = \frac{\alpha_{g,j}}{\sum_j \alpha_{g,j} V_j} \dot{M} \tag{19}$$

By substituting Eq. (16) into Eq. (19), the mass transfer rate, or mass source term, in the jth interface-cell is determined as

$$S_{\alpha_k} = \dot{m}_j = \frac{h_i}{h_{fg}} \frac{(T_{sat} - T_{l,j}) A_b \alpha_{g,j}}{\sum_j \alpha_{g,j} V_j} \tag{20}$$

where $T_{l,j}$ is the local liquid temperature at the center of mass for the jth interface-cell in the liquid temperature profile.

The energy transfer rate, or energy source term, in the jth interface-cell is obtained by multiplying Eq. (20) by h_{fg}

$$S_h = \dot{m}_j h_{fg} = \frac{h_i (T_{sat} - T_{l,j}) A_b \alpha_{g,j}}{\sum_j \alpha_{g,j} V_j} \tag{21}$$

Using this UDF of bubble condensation, this study simulates the condensing bubble with the FLUENT code. There are a few characteristics in this UDF of bubble condensation. (1) Instead of calculating the condensation rate directly, this UDF uses the condensation correlation because the use of correlation has the merit of predicting the condensation rate approximately. (2) In this UDF, IHTC is updated at each time step as the bubble behavior changes continuously. (3) IHTC is assumed to be uniform everywhere on the bubble surface but because the source terms are determined by local variables in Eqs. (20) and (21), the local condensation rate in each interface-cell is different along the surface of the bubble. (4) In this UDF, the condensation rate is not significantly affected by the cell size if the bubble velocity is predicted adequately because the main factor of calculating the IHTC is the bubble velocity.

3.3. Validation of UDF of bubble condensation

3.3.1. SNU experiment on bubble condensation

In order to validate this UDF of bubble condensation, the results of the SNU experiment on bubble condensation (Kim and Park, 2011) are used. In the experiment, the behavior of single condensing bubble was analyzed in subcooled boiling flow.

Fig. 2 shows a schematic diagram of the SNU experiment. The water flows upward and vapor bubbles are generated from the heated wall. The total length of the test channel is 1000 mm. The local liquid temperature and condensing rate are measured at 500 mm from the starting point of the heated section. The length of the test section is 30 mm and the flow channel has a square

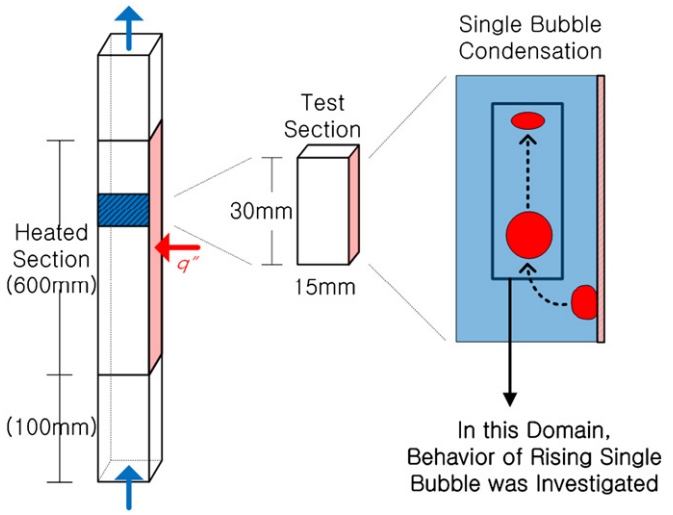

Fig. 2. SNU experiment on bubble condensation.

cross-section whose dimensions are $15 \times 15\ \text{mm}^2$. Using this facility, single condensing bubble that detached from the heated wall was investigated.

In the experiment, the procedure of the condensing bubble analysis is as follows. (1) The single rising bubble was captured constantly at regular time interval by a high-speed camera. (2) The bubble boundary was extracted using an image processing technique (Kim and Park, 2007). (3) By tracking the rising bubble, the time dependent-bubble volume, area, velocity, diameter and shape were analyzed. Finally, a condensation correlation (see Eq. (9)) was developed using the local liquid temperature and time-dependent bubble behavior.

3.3.2. Simulation procedure

The procedure of the bubble condensation simulation is shown in Fig. 3.

(1) The flow channel and meshes are generated in a three-dimensional Cartesian coordinate system using GAMBIT 2.2.30. The dimensions of the test channel are $15 \times 15 \times 30\ \text{mm}^3$ and the flow direction is upward as shown in Fig. 2. The inlet and outlet faces of the channel are modeled as the velocity-inlet and pressure-outlet, respectively. The four side walls are modeled as wall.

(2) The initial and boundary conditions such as the liquid temperature, liquid velocity and bubble region are set using UDF. When setting the initial condition, the local liquid temperature profile is specified using the temperature data measured in the SNU experiment. The local liquid velocity distribution is specified by the profile in any parabolic shape, which is determined from the average mass flow rate measured in the experiment, because the local liquid velocity was not measured in the experiment. An asymmetric bubble image was applied, which had the same volume with that of the bubble volume measured in the experiment.

(3) An adapted mesh option is applied to the bubble interface in order to better resolve the change of interface with minimal numerical cost. Generally, in the analyses of the effect of grid resolution on adiabatic bubble simulations, it has been reported that 16 CPD (Cells Per bubble Diameter) is appropriate to simulate bubble behavior with the VOF model (Bothe et al. 2006; Rabha and Buwa, 2009). However, 16 CPD cannot be maintained in bubble condensation simulations as the

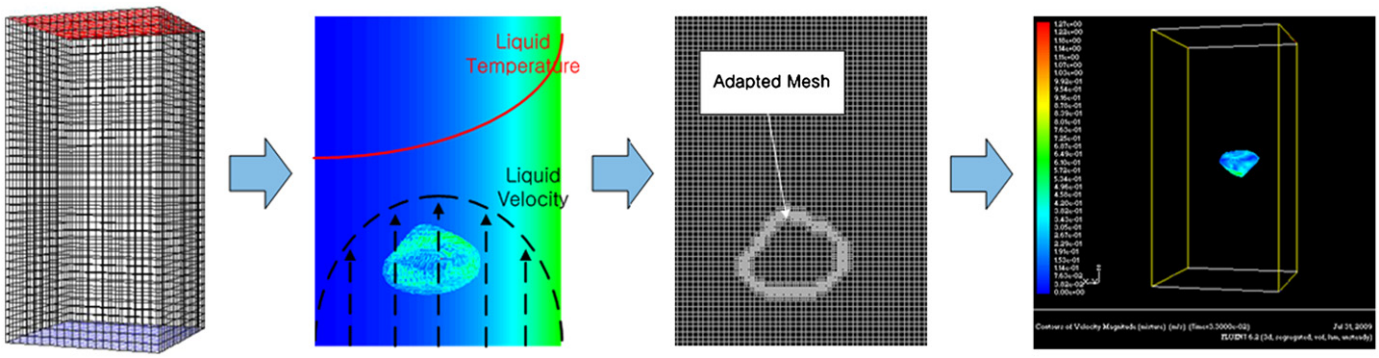

Fig. 3. Procedure of bubble condensation simulation.

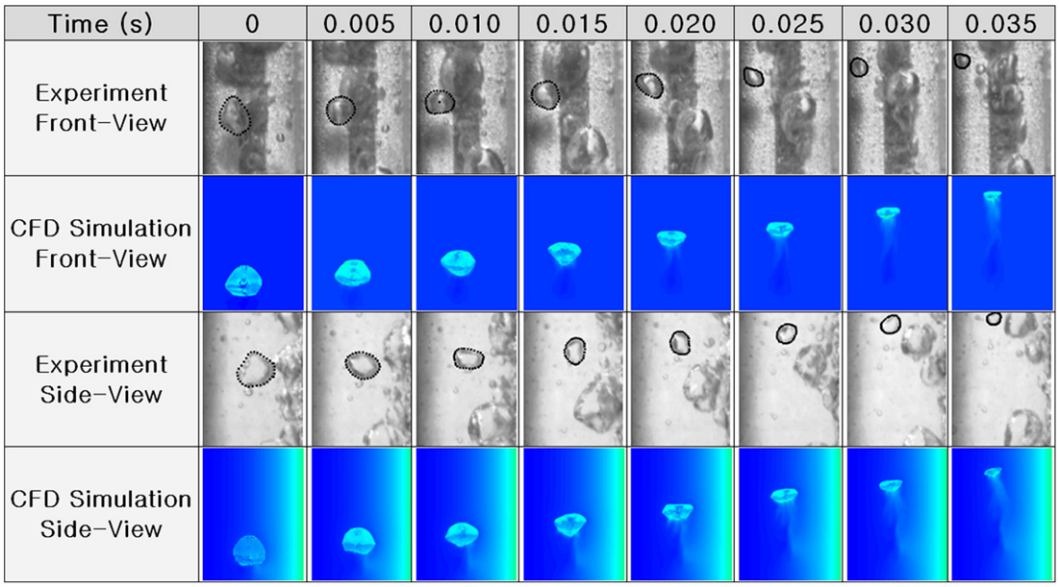

Fig. 4. Comparisons of CFD simulation and experimental results.

bubble diameter decreases. Therefore, a greater CPD is required. The adapted mesh option used in FLUENT code splits the interface-cell into quarters and improves the accuracy. To avoid excessive smearing of the interface by numerical diffusion, it is ensured that the mesh size of the interface-cell should be less than 1/16 of a diameter. In that mesh size, rich dynamic features can be captured.

(4) The condensing bubble is simulated using the VOF model coupled with the UDF of bubble condensation. The time steps used in the simulations are usually 0.00001 s.

3.3.3. *Simulation results*

Fig. 4 qualitatively shows the time-dependent behavior of the condensing bubble including features such as the bubble shape, size and interaction with the subcooled liquid. As time progresses, the vapor bubble rises up and is condensed in the subcooled flow. The asymmetric bubble shape is changed to an ellipsoidal shape. In addition to the bubble condensation, the turbulent mixing phenomenon due to the bubble behavior, which is difficult to observe in the experiment, is also observed. In the side view, hot water near the heater is mixed with cold water in the core as the rising bubble agitates the water. The differences between the numerical and experimental bubble behaviors such as bubble shape, moving distance, etc. are due to the somewhat different initial conditions; it is difficult to set the actual flow field around the experimental bubble as the initial condition. Considering the somewhat different initialization, uncertain velocity field and multi-bubble effect in the experiment, the agreement between the results may be considered reasonable.

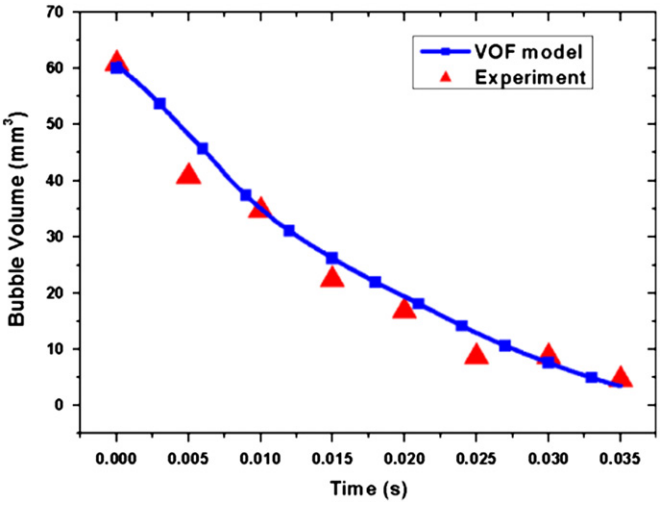

Fig. 5. Comparison of bubble volume.

Fig. 5 shows the time-dependent bubble volume. The bubble volume decreases due to condensation. The calculated result for

the condensation rate shows good agreement with the experimental data. From Figs. 4 and 5, it is concluded that the mass source term works well in the VOF model.

In the simulation of bubble condensation, emitted condensation heat is also observed. Fig. 6 shows a cross-section of the condensing bubble in Fig. 4. There are blue, green and red regions, which indicate the subcooled water, bubble interface and vapor bubble region, respectively. In this figure, it should be noted that there is a bright-blue region at the bottom of the bubble. This region indicates that the condensation heat emitted from the interface heats the subcooled water as the vapor bubble is condensed. It is concluded that the energy source term works well in the VOF model.

In Fig. 6, the temperature rise of the surrounding water due to the condensation heat is notable at the bottom of the bubble although the condensation heat is given off from all around the bubble interface. The reason is as follows. As the bubble rises up in the subcooled water, it pushes the water out thus the liquid circulation occurs around the bubble. Due to the liquid circulation, the heated water at the top of the bubble flows down along the bubble surface, and then accumulates at the bottom of the bubble. As the condensation heat is continuously transferred to the heated water at the bottom of the bubble, the temperature of the water in this region becomes higher than that of the water around the top or side region of the bubble. Therefore, high-temperature water is shown in the bottom of the bubble as thermal evidence of the condensing bubble.

4. Analysis of behavior of condensing bubble

Generally, bubble behavior can be described through the bubble size, shape, velocity, moving trajectory and interaction with liquid. A lot of numerical studies on bubble behavior have been performed by analyzing these parameters. As a result, various effects of surface tension, liquid viscosity, inertia, buoyancy, drag force, etc. on the behavior of adiabatic bubbles have been well understood. However, the understanding of the behavior of condensing bubbles is insufficient yet. Therefore, in this section, a fundamental analysis of the effects of bubble condensation on bubble behavior is performed qualitatively by comparing the behavior of condensing bubbles with that of adiabatic bubbles under various conditions.

In order to understand the effects of condensation on bubble behavior, the two-dimensional bubbles shown in Fig. 7(a), (b) and (c) were simulated in Cartesian coordinates. The analysis of the behavior of condensing bubble was first carried out at different degrees of liquid subcooling with initial bubble diameters of 2, 3 and 4 mm, respectively (see Fig. 7(a)). Here, the adiabatic bubble

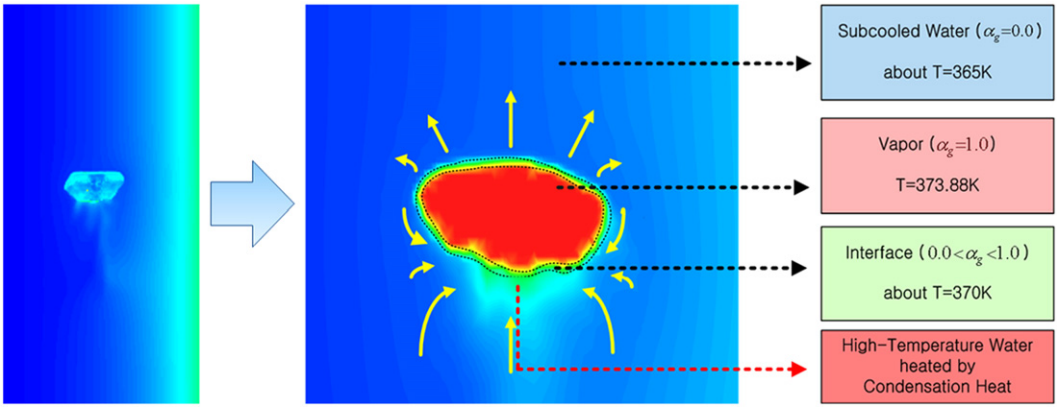

Fig. 6. Cross-section of condensing bubble in subcooled flow.

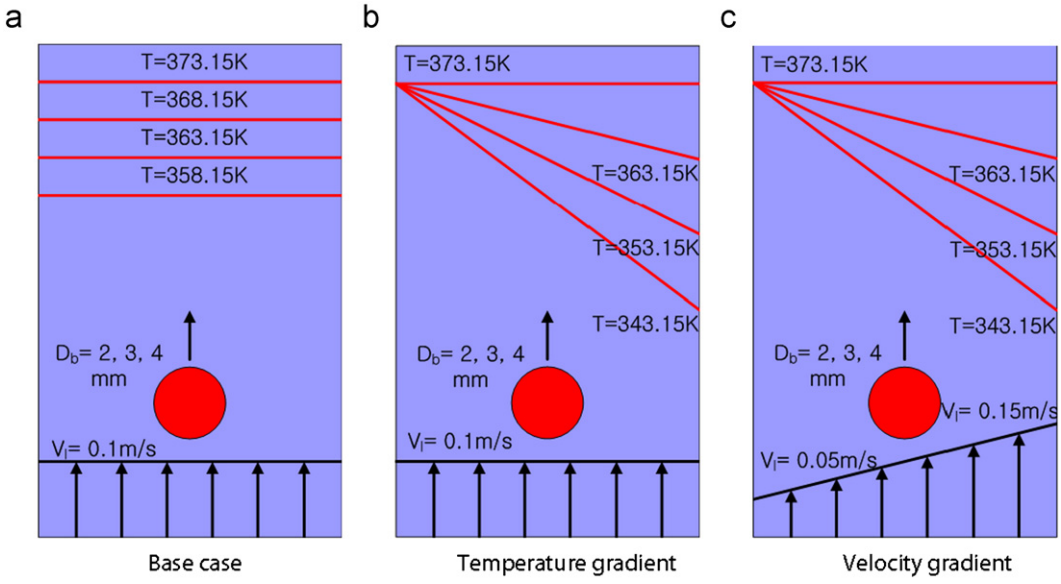

Fig. 7. Schematic diagrams of bubble condensation simulations.

simulations (T=373.15 K) are used for comparison with the condensing bubble simulations.

Fig. 8 qualitatively contrasts the time-dependent behavior of the condensing bubble with that of the adiabatic bubble. For the adiabatic-bubble simulations (see Fig. 8(a), (c) and (e)), each bubble rises up in the liquid whilst retaining its initial bubble size, and just the bubble shape is changed by the hydrodynamic force. For the smaller bubble (D_b=2 mm) in Fig. 8(a), the initial spherical bubble exhibits a slightly ellipsoidal shape as time progresses, but the deformation is negligible. However, for the larger bubbles (D_b=3, 4 mm) in Fig. 8(c) and (e), the bubble shape varies continuously from spherical to ellipsoidal, and then to hemispherical shape. From these figures, it is found that the sequence of shape changes of the adiabatic bubble varies with the initial bubble size.

In the subcooled system, on the other hand, for the 2 mm bubble in Fig. 8(b), each bubble retains a nearly spherical shape, and just the size decreases. For the 3 mm and 4 mm bubbles in Fig. 8(d) and (f), the shape of the condensing bubble changes from spherical to ellipsoidal and then returns to the spherical shape again. For the condensing bubbles, as shown in Fig. 8(d) and (f), the deformation phenomenon tends to disappear and the bubble remains nearly spherical throughout the entire lifetime (Tian et al., 2010). It is found that the deformation aspect of the condensing bubble differs from that of an adiabatic bubble. A detailed analysis of the behavior of the condensing bubble regarding the bubble velocity, rise distance and moving trajectory is described in the next part.

4.1. Effect of bubble condensation on bubble velocity and rise distance

In general, as time progresses, the rising bubble in the liquid accelerates to reach a constant terminal velocity (Clift et al. 1978) determined by the initial bubble size and properties of each

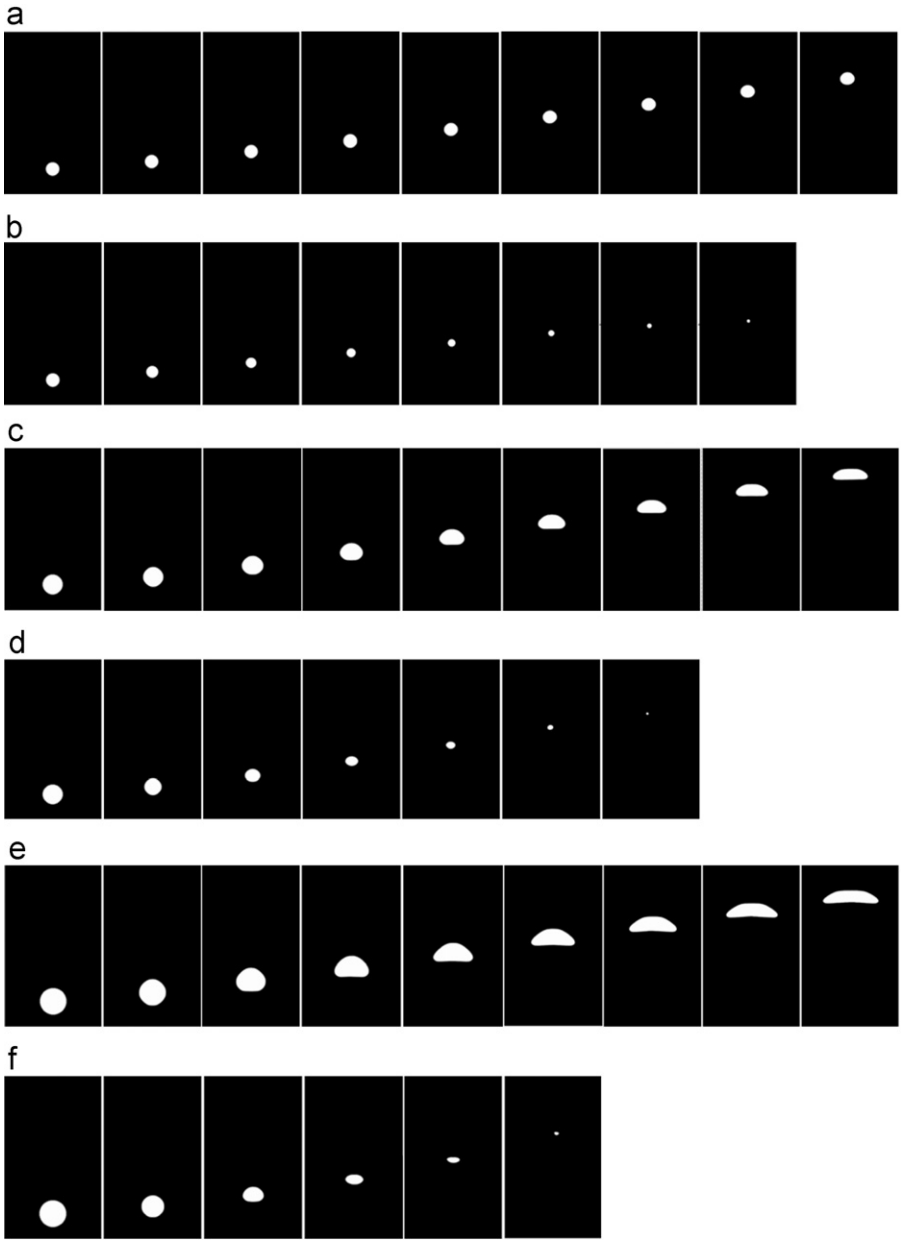

Fig. 8. Comparison of adiabatic and condensing bubble simulations. (a) Bubble Shape Sequence (D_b=2 mm, ΔT=0 K), (b) Bubble Shape Sequence (D_b=2 mm, ΔT=5 K), (c) Bubble Shape Sequence (D_b=3 mm, ΔT=0 K), (d) Bubble Shape Sequence (D_b=3 mm, ΔT=10 K), (e) Bubble Shape Sequence (D_b=4 mm, ΔT=0 K) and (f) Bubble Shape Sequence (D_b=4 mm, ΔT=15 K).

phase. However, these characteristics might be applied only to the adiabatic bubble. The rise velocity of the condensing bubble is different from that of the adiabatic bubble because the condensing bubble loses its own mass continuously.

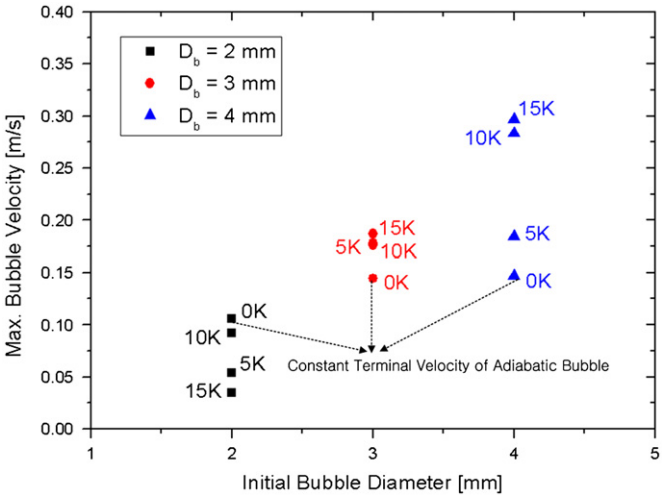

Fig. 9. Maximum bubble velocity.

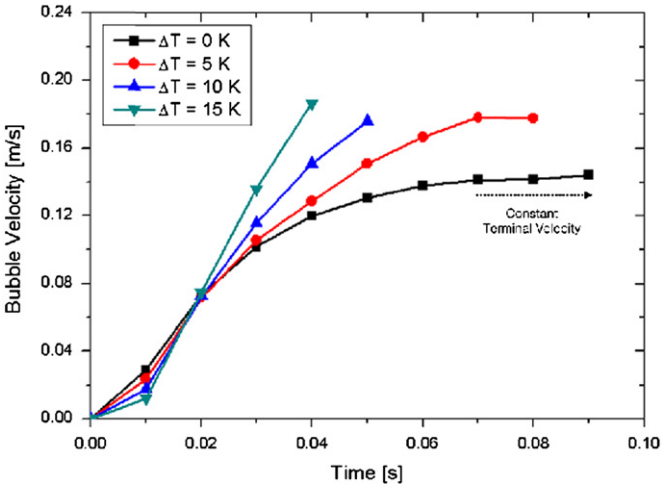

Fig. 10. Time-dependent bubble velocity (D_b=3 mm).

The effect of the bubble condensation on the bubble-rise velocity during the bubble lifetime was investigated by simulating the rise of bubbles with diameters of 2, 3 and 4 mm at different degrees of liquid subcooling (see Fig. 7(a)). The predicted terminal rise velocities were plotted as a function of the initial bubble diameter, as shown in Fig. 9. It can be seen that the condensing-bubble velocities are different from the adiabatic-bubble velocities although the initial bubble diameters are the same. For the smaller bubble (D_b=2 mm), the adiabatic bubble is faster than the condensing bubble; the adiabatic bubble reaches the terminal velocity, 0.11 m/s, but the condensing bubble disappears into the liquid before the bubble velocity reaches the terminal velocity. For the smaller condensing bubble, since the bubble lifetime is so short, it is difficult to discuss the effect of condensation on the bubble velocity. However, it can be seen that as the initial bubble size increases, the condensation effects on the bubble velocity become prominent.

Fig. 10 shows the time-dependent rise velocity of a 3 mm bubble at different degrees of liquid subcooling, representatively. Regarding larger bubbles (D_b=3 and 4 mm), the adiabatic bubble reaches the constant terminal velocity but the rise velocity of the condensing bubble increases continuously as the bubble loses its own mass continuously. As the liquid subcooling increases, due to the increase in bubble condensation, the bubble velocity increases rapidly and the final velocity of the condensing bubble becomes higher than the terminal velocity of the corresponding adiabatic bubble.

These phenomena might be explained by the following reasons. Fig. 11 shows the relation between forces acting on the bubble and the bubble velocity. When simplifying the relation, it could be assumed that the increase of bubble velocity is determined by the force balance of the drag force and the buoyancy force. For the adiabatic bubble, the buoyancy force is constant but the drag force increases due to the increase of the bubble frontal area through the shape deformation. As the time progresses, the net force acting on the adiabatic bubble decreases, finally, the bubble velocity reaches its terminal velocity. However, for the condensing bubble, the buoyancy force decreases due to the decrease of the bubble volume but the drag force also decreases caused by the decrease of bubble frontal area; there is just a slight change in the bubble shape due to the increase in the influence of the surface tension force, which is always trying to maintain a shape that has minimum surface energy. To conclude, the buoyancy force is larger than the drag force meaning that the net force stays positive; therefore the bubble velocity increases continuously.

The bubble condensation decreases the bubble lifetime and, by extension, the bubble rise distance as well. Fig. 12 shows the

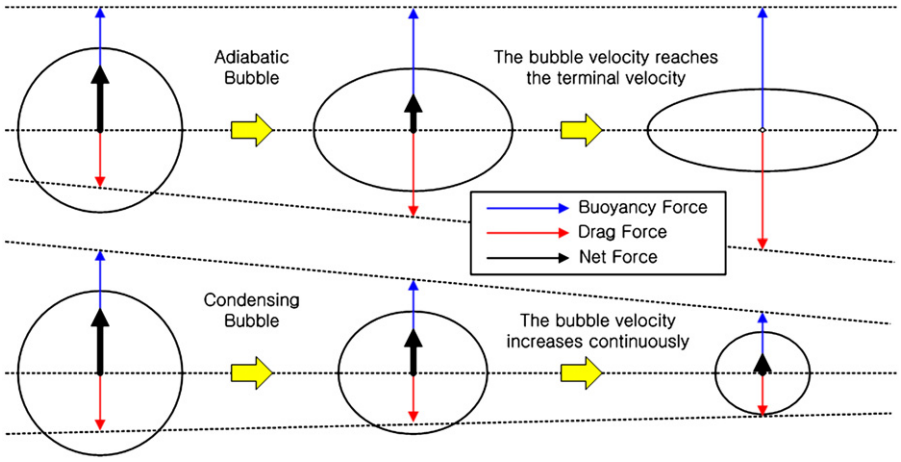

Fig. 11. Force balance diagram for adiabatic and condensing bubble.

time-dependent positions of 4 mm bubbles at different levels of liquid subcooling. Each bubble is illustrated with a time interval of 0.01 s. It can be found that the bubble rise distance is reduced because of the shorter lifetime as the liquid subcooling increases. However, in this figure, the last position of each condensing bubble should be noted. During the same amount of time, the rise distance of the condensing bubble is longer than that of the adiabatic bubble. This is because the bubble velocity increases due to the condensation as mentioned earlier. After the medium stage of the bubble lifetime, the condensing bubble accelerates so that the bubble moves faster and then disappears. This phenomenon is particularly noticeable in a larger bubble with a longer lifetime wherein the bubble accelerates sufficiently.

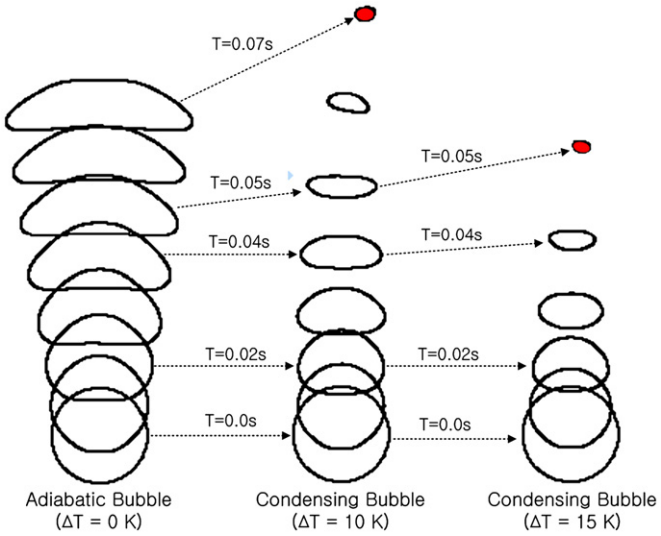

Fig. 12. Bubble rise history (D_b=4 mm).

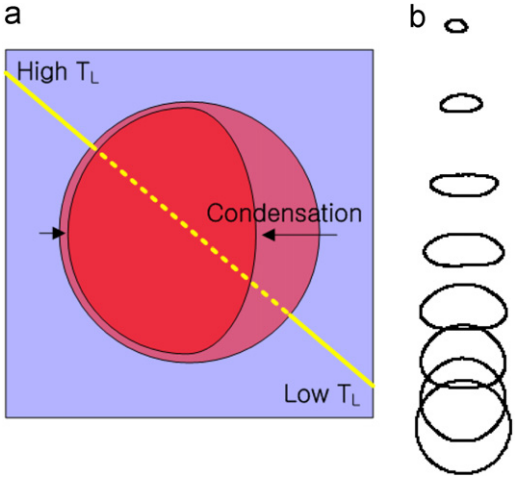

Fig. 13. Moving trajectory and bubble deformation. (a) Speculative Bubble Deformation and (b) D_b=4 mm, ΔT=10 K.

4.2. Effect of bubble condensation on bubble moving trajectory

In order to understand the effects of the difference in the local condensation rate along the bubble surface on the bubble moving trajectory, the two-dimensional bubbles shown in Fig. 7(b) were simulated in the liquid with a linear temperature gradient. As shown in Fig. 13(a), it is easily guessed that the condensing rate on the right side of the bubble is larger than that on the left side of the bubble due to the local liquid temperature difference thus the bubble shape is changed into an asymmetrical shape and then the moving trajectory is also changed.

However, the effect of the difference in the local condensation rate seems to be negligible in these bubble simulations. Fig. 13(b) shows representative simulation results for a condensing bubble in liquid with a temperature gradient. There is no asymmetrical change in shape and the condensing bubbles rise nearly upright. Although, in this study, the spatial distribution of IHTC along the bubble surface is not taken into consideration, these results show that the difference of local IHTC along the bubble surface does not significantly affect the behavior of the condensing bubble. Therefore, it could be concluded that the UDF of bubble condensation proposed in this study does not oversimplify the problem.

In order to investigate the effect of condensation on the bubble moving trajectory, the two-dimensional bubbles shown in Fig. 7(c) were simulated in the liquid with a linear velocity gradient. The calculated moving trajectories and bubble shapes in liquid with a velocity gradient are shown in Fig. 14.

For the 2 mm bubble in Fig. 14(a), the adiabatic bubble moves along more or less sinuous paths but the change in the rise trajectory is hardly noticed compared with those of the 3 mm and 4 mm bubbles. It might be because the bubble moving trajectory in the liquid depends on the bubble shape that is deformed by the interaction with the surrounding liquid. For the 2 mm bubble, since the bubble size is so small the effect of surface tension is large enough to prevent a shape change. Therefore, the smaller bubble rises almost upright despite the existence of a liquid velocity gradient.

On the other hand, for larger bubbles (D_b=3 and 4 mm), prominent changes are observed for both the moving trajectory

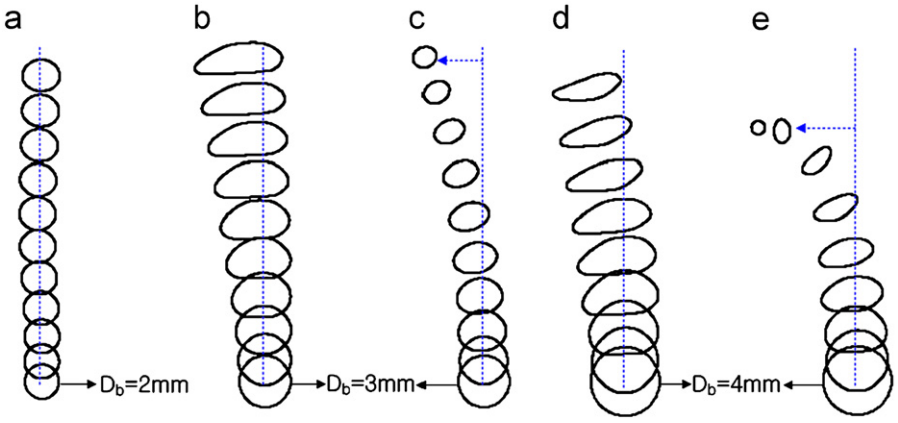

Fig. 14. Bubble rise history. (a) ΔT=0 K, (b) ΔT=0 K, (c) ΔT=5 K, (d) ΔT=5 K and (e) ΔT=10 K.

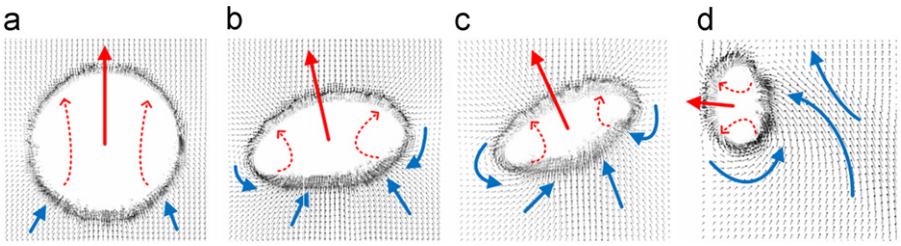

Fig. 15. Velocity distribution around condensing bubble (D_b=4 mm, ΔT=10 K). (a) t=0.01 s, (b) t=0.03 s, (c) t=0.05 s and (d) t=0.07 s.

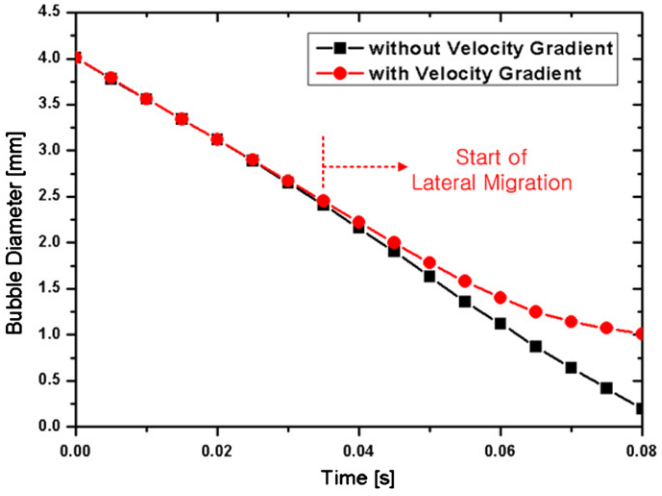

Fig. 16. Comparison of bubble diameter (D_b=4 mm, ΔT=10 K).

and the bubble shape. As shown in Fig. 14(b) and (d), the calculated bubble shapes change from spherical to wing-shaped. For the condensing bubble, the shape changes from spherical to wing and finally to ellipsoidal (see Fig. 14(c) and (e)). In addition, as the liquid subcooling increases, the bubble migrates more toward a lower velocity region (see Figs. 7(c) and 14(e)). It can be seen that condensation accelerates the lateral migration of the bubble in liquid with a velocity gradient.

Fig. 15 shows a time history of the velocity distribution around the fluctuating bubble with an initial bubble diameter of 4 mm at a liquid subcooling of 10 K (see Fig. 14(e)). The condensing bubble deformed by the hydrodynamic force, the internal circulation due to momentum transfer across the vapor–liquid interface, and the liquid circulation around the bubble are observed. It can be seen that the velocity field in the bubble determined by the interaction with the surrounding liquid induces lateral migration through an asymmetrical deformation of the bubble shape.

Fig. 16 shows a representative, time-dependent bubble diameter in liquid with a temperature gradient. Since the 4 mm bubble rises upright in liquid without a velocity gradient (see Fig. 13(b)), the bubble size decreases nearly linearly. However, the 4 mm bubble in liquid with a velocity gradient migrates toward the higher-temperature region in the liquid (see Figs. 7(c) and 14(e)) thus the bubble lifetime becomes longer due to the decreased condensation rate. Consequently, it is found that the lateral migration of the bubble significantly affects the bubble lifetime in liquid with a temperature gradient.

5. Conclusion

In this study, the behavior of condensing bubble was numerically investigated using VOF model. In order to simulate the condensing bubble in CFD code, the bubble condensation was modeled first using the UDF in FLUENT code. For the validation of the UDF of bubble condensation, the predictions from the 3D simulation were compared with the results of the SNU bubble condensation experiment. The simulation results predicted the behavior of an actual condensing bubble well. It can be concluded that the VOF model coupled with the UDF of bubble condensation proposed in this study can simulate the complex behavior of the condensing bubble.

Furthermore, the behavior of condensing bubbles was investigated qualitatively under various conditions. The key conclusions regarding the effects of bubble condensation on bubble behavior are as follows.

1. The bubble condensation increases the bubble velocity.
2. As the condensation rate increases, the rise distance of the condensing bubble is reduced due to the shorter lifetime but the condensing bubble travels longer distance than the adiabatic bubble does during the same amount of time.
3. The bubble condensation accelerates the lateral migration of the bubble in liquid with a velocity gradient, which in turn affects the bubble lifetime in liquid with a temperature gradient.

The results of this study show the effect of condensation on bubble behavior well. It is confirmed that the behavior of the condensing bubble, which is difficult to measure in experimental researches, is different from that of the adiabatic bubble. However, it should be noted that the behavior of condensing bubbles such as bubble velocity, rise distance and moving trajectory reported here were qualitatively investigated with 2D simulation. Therefore, it is recommended that future research focuses on 3D simulation to quantify the robustness of VOF model for the analysis of the behavior of condensing bubbles. Systematic investigations of the behavior of condensing bubbles with 3D simulation and appropriate experimental validation will be useful to improve the understanding of the two-phase subcooled system.

Nomenclature

A	bubble surface area (mm^2)
C_p	specific heat (J/kgK)
D_b	initial bubble diameter (mm)
D_s	Sauter diameter (mm)
E	energy (J)
F	force (N)
h_i	interfacial heat transfer coefficient (J/m^{2}K)
h_{fg}	latent heat (J/kg)
Ja	Jacob number
k	thermal conductivity (J/mK)
Nu_c	condensate Nusselt number
Pr	Prandtl number
Re_b	particle (bubble) Reynolds number
S	source term

T	temperature (K)
t	time (s)
U_b	bubble velocity (m/s)
U_{rel}	bubble relative velocity (m/s)
V_b	bubble volume (mm^3)
V_j	cell volume (m^3)
x	x-coordinate
x_{CM}	center of mass
y	y-coordinate
z	z-coordinate

Greek letters

α_g	vapor volume fraction
μ	viscosity
ρ	density (kg/m^3)

Subscripts

j	jth cell
l	liquid
sat	saturation
sub	subcooled

References

Annaland, M.S., Deen, N.G., Kuipers, J.A.M., 2005. Numerical simulation of gas bubbles behavior using a three-dimensional volume of fluid method. Chemical Engineering Science 60, 2999–3011.

Bothe, D., Schmidtke, M., Warnecke, H.J., 2006. VOF-simulation of the rise behavior of single air bubbles in linear shear flows. Chemical Engineering and Technology 29, 1048–1053.

Chen, L., Li, Y., 1998. A numerical method for two-phase flows with an interface. Environmental Modeling & Software 13, 247–255.

Clift, R., Grace, J.R., Weber, M.E., 1978. Bubbles, Drops and Particles. Academic Press.

Fluent 6.0 Users Guide Documentation, 2001. Fluent Inc., Lebanon, New Hampshire.

Gopala, V.R., Wachem, B.G.M., 2008. Volume of fluid methods for immiscible-fluid and free-surface flows. Chemical Engineering Journal 141, 204–221.

Hirt, C.W., Nichols, B.D., 1981. Volume of fluid (VOF) method for the dynamics of free boundaries. Journal of Computational Physics 39, 201–225.

Kim, S.J., Park, G.C., 2007. Development of an orthogonal double-image processing algorithm to measure bubble volume in a two-phase flow. Nuclear Engineering and Technology 39 (4), 313–326.

Kim, S.J., Park, G.C., 2011. Interfacial heat transfer of condensing bubble in subcooled boiling flow at low pressure. International Journal of Heat and Mass Transfer 54, 2962–2974.

Krishna, R., Baten, J.M., 1999. Rise characteristics of gas bubbles in a 2D rectangular column: VOF Simulations vs experiments. International Communications in Heat and Mass Transfer 26, 965–974.

Lörstad, D., Fuchs, L., 2004. High-order surface tension VOF-model for 3D bubble flows with high density ratio. Journal of Computational Physics 200, 153–176.

Rabha, S.S., Buwa, V.V., 2009. Volume-of-fluid (VOF) simulations of rise of single/multiple bubbles in sheared liquids. Chemical Engineering Science 65, 527–537.

Taha, T., Cui, Z.F., 2006. CFD modeling of slug flow in vertical tubes. Chemical Engineering Science 61, 676–687.

Tian, W.X., Ishiwatari, Y., Ikejiri, S., Yamakawa, M., Oka, Y., 2010. Numerical computation of thermally controlled steam bubble condensation using Moving Particle Semi-implicit (MPS) method. Annals of Nuclear Energy 37, 5–15.

Tomiyama, A., Sou, A., Minagawa, H., Sakaguchi, T., 1991a. Numerical analyses of a single bubble with VOF method. Transactions of the Japan Society of Mechanical Engineers 57-539, 1–7.

Tomiyama, A., Sou, A., Matsui, M., Sakaguchi, T., 1991b. Analyses of bubble behavior with the volume of fluid method. In: Proceedings of the Fluids Engineering Conference '91, JSME, vol. 910-50, pp. 341.

Tomiyama, A., Iztok, Z., Akira, S., Tadashi, S., 1993. Numerical analysis of bubble motion with the VOF method. Nuclear Engineering and Design 141, 69–82.

Wachem, B.G.M., Schouten, J.C., 2002. Experimental validation 3-D Lagrangian VOF model: bubble shape and rise velocity. AIChE Journal 48, 2744–2753.